

# Advanced Image Formation and Processing of Partial SAR Data

Shaun I. Kelly, Chaoran Du, Gabriel Rilling, Mike E. Davies

**Abstract**—We propose an advanced synthetic aperture radar (SAR) image formation framework based on iterative inversion algorithms that approximately solve a regularised least squares problem. The framework provides improved image reconstructions, compared to the standard methods, in certain imaging scenarios, e.g. when the SAR data is under-sampled. Iterative algorithms also allow prior information to be used to solve additional problems such as the correction of unknown phase errors in the SAR data. Though, for an iterative inversion framework to be feasible, fast algorithms for the generative model and its adjoint must be available. We demonstrate how fast,  $N^2 \log_2 N$  complexity, (re/back)-projection algorithms can be used as accurate approximations for the generative model and its adjoint, without the limiting geometric approximations of other  $N^2 \log_2 N$  methods, e.g. the polar format algorithm (PFA). Experimental results demonstrate the effectiveness of our framework using publicly available SAR datasets. The `Matlab/C` code implementation of the fast (re/back)-projection algorithms used in this paper has been made available.

## I. INTRODUCTION

Synthetic aperture radar (SAR) is an active ground imaging system based on coherent processing of multiple radar echoes acquired along the path of a moving platform (aircraft or satellite). Assuming free space propagation of the radar waves, scalar wavefields, no mobile targets and single bounce scattering by ground reflectors, the map from the SAR image to the received radar echoes can be modelled as linear. When everything is discretised this map can be represented by an observation matrix  $\Phi$ . Traditional processing of the SAR data involves the approximation of the pseudo-inverse  $\Phi^\dagger$  by the adjoint  $\Phi^H$ , which is commonly referred to as the back-projection operator. This leads to the *filtered back-projection* reconstruction which adds some linear filter to the adjoint to make it closer to  $\Phi^\dagger$ . This provides good quality images when the SAR data is densely sampled and the image is reconstructed at its native resolution, defined by the bandwidth of the emitted radar signals and the length of the synthetic aperture.

Without further approximations of the SAR model and a straightforward implementation, the back-projection operator  $\Phi^H$  is rather slow with a complexity of  $\mathcal{O}(N^3)$  when processing  $N$  radar echoes of  $N$  samples each. Because of low computational resources — especially on mobile platforms — that algorithm is often replaced by an approximation referred to as the Polar Format Algorithm (PFA). Assuming constant terrain elevation and flat wavefronts (far-field scenario), this algorithm reduces the complexity to  $\mathcal{O}(N^2 \log N)$ . This is the same complexity as a 2D-FFT and the PFA can furthermore be implemented nearly as fast using nonuniform FFT algorithms [1]. Using techniques from the tomography literature it has been shown that the operators  $\Phi$  and  $\Phi^H$  can also be implemented in  $\mathcal{O}(N^2 \log N)$  iterations without using the approximations of the PFA [2], [3]. Also, more recently another approach has been shown to provide similar speedup with some additional theoretical guarantees regarding the quality of the reconstruction [4]. Despite being slower than the PFA, these fast algorithms make it possible to use these more accurate operators in practice. This results in enhanced image quality as well as more versatility, allowing, for instance, more general flight paths and the ability to reconstruct images on non flat terrain if an elevation map is known.

In order to improve further the image quality, one can also use iterative algorithms to compute the pseudo-inverse  $\Phi^\dagger$  rather than use the back-projection approximation. Because the matrix  $\Phi$  is generally very large, direct computation of the pseudo-inverse is not practical. Instead, it can be computed by finding the minimum of the least squares

$$f = \underset{\tilde{f}}{\operatorname{argmin}} \|y - \Phi \tilde{f}\|_2^2, \quad (1)$$

where  $f$  stands for the SAR image (represented as a vector) and  $y$  for the SAR data. This can be done very efficiently using a conjugate gradient which requires several iterations of the operators  $\Phi$  and  $\Phi^H$ . As will be shown in the paper the number of iterations does not need to be large to produce a good quality image. This makes such iterative methods affordable provided fast implementations of the operators  $\Phi$  and  $\Phi^H$  are available. When densely sampled SAR data are available, such iterative methods only provide minor image quality improvements. However, they become increasingly necessary when there is missing data.

In a variety of situations it is desirable to produce images from only partial SAR data. Missing data patterns can take various forms:

- *missing radar echoes at some locations along the synthetic aperture.* This corresponds to temporary interruptions of the acquisition of SAR data along the trajectory, which typically results from the need to use the radar antenna for other tasks. Examples of applications are collecting SAR data from another ground patch (as in ScanSAR), alternating polarisations of the radar waves to obtain images at multiple polarisations, or scanning the air space in a military context [5].
- *missing frequency bands in the radar signal.* This occurs in the case of ultra wide band SAR where the desired band of the radar contains sub-bands that are saturated by other communications systems or in which transmission is not allowed [6].
- *arbitrary missing data.* This may occur if one throws away samples from the acquired data to reduce the amount of data stored on the acquisition platform. This provides some trivial compression of the data which may prove useful on platforms with low computational resources and storage capacities such as satellites [7], [8].

In any of these missing data scenarios, standard reconstruction through back-projection amounts to assuming that the missing data are zeros. It produces undesirable artifacts that may drastically reduce the image quality and make further exploitation impossible. In order to improve the image quality the observation matrix  $\Phi$  must be properly inverted. Because of the missing data, the problem is ill-posed and further assumptions are required to define a unique solution. A standard signal processing approach is to solve a penalised least-squares problem

$$f = \underset{\tilde{f}}{\operatorname{argmin}} \|y - \Phi \tilde{f}\|_2^2 + \lambda L(\tilde{f}), \quad (2)$$

where  $L$  stands for a regularisation function. Typical examples of  $L$  are  $\ell_p$  norms,  $L(\tilde{f}) = \|\tilde{f}\|_p^p$ , and such penalties with  $p \leq 1$  have been considered for SAR in the context of superresolution [9], [10] and more recently for processing partial SAR data [11], [12]. Other

regularisation functions such as total variation norms have also been considered for speckle reduction [9]. The use of  $\ell_p$  norms has recently received considerable attention in the context of the emerging field of *compressed sensing* (CS) [13], [14] which properly justifies their use (especially in the case  $p = 1$ ) when the SAR image can be modelled as *sparse*.

CS has also motivated the development of several fast solvers for the  $\ell_1$  penalised least squares problem (or one of its equivalent constrained optimisation forms) [15], [16]. Like the conjugate gradient solver for the standard least squares problem (1), these solvers require the iteration of the operators  $\Phi$  and  $\Phi^H$  and are therefore prohibitively slow unless fast implementations of the operators are available. When these are available, such algorithms may be affordable and produce good quality images with only a small number of iterations.

In this paper, a framework for SAR processing using iterative methods is described and it is shown that advanced image formation steps such as autofocus or the ability to reconstruct images of non-flat terrain from arbitrary trajectories fit naturally within this framework. Its usefulness is also demonstrated when only partial SAR data are available and quantified through automatic target recognition performance analysis. For simplicity, we only consider monostatic SAR (collocated receiver and emitter) in the *spotlight mode* where the radar beam is focused on the same area for all the emitted radar waves. However it is important to note that the framework is just as applicable to any SAR acquisition mode.

We start off with an introduction to SAR in section II. In section III, the iterative reconstruction framework is introduced and an example of fast re/back-projection algorithm is presented. Finally section IV focuses on the application to partial data scenarios. Open source `Matlab/C` codes for the algorithms described in this paper are available from [?].

## II. SYNTHETIC APERTURE RADAR

### A. SAR imaging geometry

In mono-static spotlight-mode SAR, a received signal after it has been dechirped (mixed with a delayed version of the input signal and low-pass filtered) is given by equation (3) [17].

$$C_\theta(t) = \int_{-L}^{+L} p_\theta(u)P(u) \exp\left\{-j\frac{2u}{c}(\omega_0 + 2\alpha(t - \tau_0))\right\} du \quad (3)$$

for

$$-\frac{T}{2} + \frac{2(R_\theta + L)}{c} \leq t \leq \frac{T}{2} + \frac{2(R_\theta - L)}{c}$$

Where:  $\omega_0$  is the carrier frequency,  $2\alpha$  is the chirp rate,  $T$  is the chirp duration,  $L$  is the radius of the spotlighted region,  $u$  is distance in the direction of the transmitted signal with reference to the spotlighted scene centre,  $\tau_0 = 2R_\theta/c$ ,  $R_\theta$  is the distance to the spotlighted scene centre and  $p_\theta(u)$  is the sum of scene reflectivities  $f(\vec{X})$  at distance  $R_\theta + u$  from the antenna and is given by

$$p_\theta(u) = \int_S \delta(\|\vec{X}_\theta - \vec{X}\|_2 - (R_\theta + u)) \cdot f(\vec{X}) dS \quad (4)$$

Where:  $\vec{X} = (x, y, z(x, y))$  is a point on the scene surface,  $\delta$  is the Dirac function and  $\vec{X}_\theta$  is the antenna's position for each chirp.

$P(u)$  is a phase error term, which is a result of the dechirping operation, and is given by

$$P(u) = \exp\left\{j\alpha\left(\frac{2u}{c}\right)^2\right\} \quad (5)$$

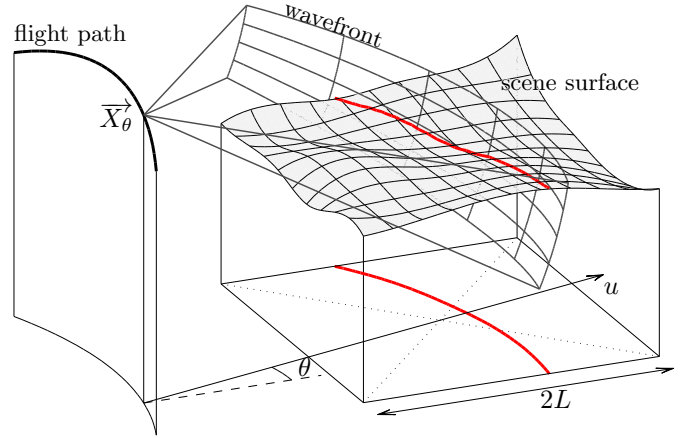


Fig. 1. Data acquisition geometry for spotlight-mode SAR given by equation (3). The red line shows the intersection of the wavefront and scene surface at a distance  $R_\theta + u$  from the antenna, the integral along this line is given by equation (4)

The set of received signals  $C_\theta$  is referred to in the SAR literature as a phase history. Observe that the received signal for each chirp, given by equation (3) (ignoring  $P(u)$ ), is the spatial Fourier transform of the projected scene reflectivities. Since  $P(u)$  is deterministic, in practice this term can be removed as a pre-processing step or ignored if negligible. The discrete version of this equation is the re-projection matrix and its adjoint is the back-projection matrix.

In (4), it is worth pointing out that the altitude of each point of the scene  $z(x, y)$  is assumed to be known. This implies that a precise elevation map of the target area, including e.g. buildings and vehicles, is required to implement the (re/back)-projection operators accurately. Such a precise elevation map is generally not known and only a coarse scale elevation map may be available. In its absence, it is common to just assume flat terrain. However, if the scene is not flat enough, this leads to distortions of the image — areas at higher altitude appear closer — and possible defocussing which results in loss of resolution [3].

### B. SAR image properties

1) *Statistical properties*: As the output of a coherent imaging system, SAR images are corrupted by speckle noise. A common model explaining the latter is based on the fact that pixels of the SAR image, at its native resolution, are typically large compared to the wavelength of the radar signal. Under this assumption, a pixel of the image can be modelled as the sum of a large number of sub-pixel objects. Each of these objects reflects a fraction of the electromagnetic energy towards the SAR acquisition platform which can be modelled through a complex-valued reflection coefficient. The value a pixel of the SAR image is then the coherent sum of these sub-pixel reflectivities. Depending on the sub-pixel characteristics of the surface of the scene, these sub-pixel reflectivities may interfere in different ways:

- *random interference*. If the surface is rough at the scale of the wavelength, it can be modelled as a large number of *independent* sub-pixel objects. The sum of the reflectivities is then a complex-valued Gaussian random variable with iid real and imaginary parts. Moreover, for two adjacent pixels, the sub-pixel objects can be assumed independent. This leads to a multiplicative iid complex Gaussian noise model for the complex-valued image at such locations, that is often referred to as *speckle* noise.

- *constructive interference*. If the surface is smooth, it can be modelled as sub-pixel objects with similar characteristics which may interfere constructively. This leads to specular reflection effects and, unless the surface is perpendicular to the incident wave propagation direction, only a very small fraction of the electromagnetic energy is reflected towards the SAR acquisition platform. An important special case is corner reflection where the radar wave bounces on faces of a corner and is massively reflected towards the acquisition platform. Such corner objects are common in man-made structures or vehicles and lead to very high magnitudes for the corresponding pixels of the SAR image, typically  $10^3$  times larger than the magnitude of pixels with random interference. Specular reflection is typically dominant in urban areas [18] and corner reflection accounts for most of the very bright pixels.

### C. SAR image model

In a typical SAR image, most pixels can be modelled as the result of random sub-pixel interference, and only a small number as constructive interference leading to very bright pixels. In order to understand the behaviour of the algorithms described in the next sections, it is convenient to split the image into these two parts

$$f = f_s + f_{bg}, \quad (6)$$

with  $f_s$  corresponding to the few very bright pixels and  $f_{bg}$  to the “background” lower reflectivity pixels contaminated by speckle noise.

Viewed as a whole, most of the SAR image contains multiplicative speckle noise and can therefore be modelled as nonstationary complex Gaussian white noise. In terms of information content, this means that the complex-valued SAR image has a very high entropy and therefore a very low compressibility. In particular it *cannot* be modelled as sparse in any dictionary which precludes the use of compressed sensing ideas to recover the full SAR image, including the speckle noise, from partial SAR data.

However, the part corresponding to the few very bright pixels  $f_s$  is clearly *sparse* in the image domain and its non-zero values are typically much larger than the values of  $f_{bg}$ . If one is interested in recovering those bright pixels, the rest of the image can be treated as noise with a reasonable signal to noise ratio. This suggests that it is a priori possible to use compressed sensing to recover those bright pixels, even from very incomplete SAR data. In practice, such bright pixels are typically related to man-made structures or vehicles and are therefore very relevant to surveillance and military applications.

## III. ITERATIVE IMAGE FORMATION FRAMEWORK

In this section we will introduce an iterative image formation framework using fast (re/back)-projection operators. We will show that an iterative framework can improve image reconstructions with only a small number of iterations in certain imaging scenarios, e.g. an irregularly sampled phase history.

### A. Fast (Re/Back)-projection

There has been a number of proposed algorithms for reducing the computational complexity of (re/back)-projection operators to  $\mathcal{O}(N^2 \log_2 N)$  in the last decade. These fast algorithms reduce complexity by exploiting redundancy in the (re/back)-projection operators, e.g. [19] and [2]. In our framework we have used the latter algorithm which exploits the operator redundancy through a divide and conquer approach.

It is well known that the range resolution  $\rho_r$  and cross-range resolution  $\rho_a$  in a spotlight-mode SAR system are approximately

given by  $c/2B$  and  $\lambda_{min}/2\Delta\theta$  respectively [20]. Where:  $B$  is the bandwidth of the linear chirp,  $\lambda_{min}$  is the smallest wavelength of the chirped signal and  $\Delta\theta$  is the angular extent of the synthetic aperture. Therefore, both the range and cross-range sampling periods are linearly proportional to the scene size for constant range and cross-range resolutions.

This property lends itself to a divide and conquer strategy where the original scene is recursively split into smaller sub-scenes in a quadtree structure. For simplicity, we will describe the fast re-projection algorithm but the implementation of the adjoint is straightforward. Using the quadtree structure, standard re-projection is performed on all of the small sub-images at their required sampling rate, which is much less than that of the full scene. The re-projected data for each sub-scene is then radially Fourier transformed to produce a phase history. The phase histories can then be recursively combined up the quadtree, using low-pass upsampling, to produce a single phase history for the whole scene. If the original scene is split into sub-scenes of just one sample, the computational complexity of the algorithm becomes  $\mathcal{O}(N^2 \log_2 N)$ .

Critically, the fast (re/back)-projection algorithms approach the same complexity as the standard Fourier methods without being compromised by the same assumptions on the SAR acquisition geometry. The implementation of the fast re-projection algorithm used in our framework combines four sub-scene phase-histories at each stage of the recursion with the following steps:

- 1) 2D low-pass upsample the sub-scene phase histories by a factor two in range and cross-range using fast filtering in the Fourier domain
- 2) modify the upsampled phase histories’ scene centres  $\vec{rX}_c$  to a combined scene center  $\vec{X}_c$  by multiplying the phase histories by  $\exp\left\{-j\frac{2}{c}(\omega_0 + 2\alpha(t - \tau_0))(\|\vec{rX}_c - \vec{X}_\theta\|_2 - \|\vec{X}_c - \vec{X}_\theta\|_2)\right\}$
- 3) sum sets of four upsampled phase histories

In a practical implementations the recursion will not continue down to the single pixel stage. This is because the computational requirements of upsampling the phase histories when the sub-scenes are small becomes more computationally expensive than the two times speed up achieved at each stage of recursion.

To demonstrate the computational advantages of fast (re/back)-projection, Table I shows image formation times in seconds for  $N \times N$  scenes and phase histories using: standard back-projection (BP), fast back-projection (Fast BP), a non-uniform FFT implementation of the polar format algorithm (PFA), an iterative approximation of the pseudo inverse ( $\Phi^\dagger$ ) and an iterative approximation of the  $\ell_1$  regularised least squares ( $\ell_1$  reg. LS). Formation times were measured on a single core of a 2.5GHz Intel Xeon processor. The BP and PFA algorithms were both implemented in C code.

The recursive segmentation part of the Fast BP algorithm was implemented in Matlab code, with  $\log_2 N - 6$  levels of recursion. For higher levels of recursion, computation times started to increase. At the final level of recursion, the back-projection of the sub-scenes used the BP C code. If the segmentation part was also implemented in C code, reduced computation times would be expected for higher levels of recursion.

The approximate pseudo inverse was computed using 10 iterations of LSMR [21], with fast (re/back)-projection operators. Notice, the approximate pseudo inverse takes just over 20 times that of a single fast back-projection reconstruction. This is because the main computational burden of LSMR is a single re-projection and back-projection operation at each iteration.

The approximate  $\ell_1$  regularised least squares was computed using 10 iterations of GPCR [15], with fast (re/back)-projection operators. It has slightly higher reconstruction times than the approximate pseudo

inverse though its main computational burden is still a single re-projection and back-projection operation per iteration.

For both iterative algorithms, more than 10 iterations does not visually improve the image quality, see figure 3(d).

TABLE I  
IMAGE FORMATION TIMES (SECONDS)

N	BP	Fast BP	PFA	$\Phi^\dagger$	$\ell_1$ reg. LS
256	2.50	1.06	0.11	22.54	26.46
512	20.01	5.08	0.60	108.76	130.17
1024	157.32	24.87	5.55	534.40	714.05
2048	1254.48	118.69	38.19	2537.71	3574.87

### B. Digital Elevation Maps

In standard Fourier-based techniques the scene surface is assumed to be flat. In certain cases though this assumption may not be true. Topographical variations of the scene surface can cause blurring and relative distance between objects in the image to become inaccurate. These undesirable effects can be corrected using knowledge of the scene's topographical variations in the form of a Digital Elevation Map (DEM). In Fourier-based methods, corrections are added as a post-processing step. Using (re/back)-projection, DEMs can be included with no additional computational cost.

### C. Irregular Sampling

An example of a scenario where the standard direct SAR inversion problem breaks down is an irregularly sampled phase history. Under these sampling conditions the filtered adjoint, the standard SAR inversion method, is no longer an accurate surrogate for the inverse operator. The reason it is not an accurate surrogate is due to an essential interpolation step in the filtered adjoint, irregular samples must be interpolated to a regular sampling grid in any filtered adjoint type inversion algorithm, e.g. back-projection. Interpolation is easily performed from dense regularly sampled grids to irregularly sampled grids but not the other way around. Iterative algorithms can avoid problems due to interpolation by solving the pseudo inverse.

Figure 3 shows two reconstructions from the same phase history that have been irregularly sampled in cross-range with a mean spacing being at the Nyquist rate. The irregularly sampled phase history was simulated synthetically using the fast re-projection algorithm on a reconstructed SAR image. The SAR image was reconstructed from the publicly available Gotcha data set [22]. The back-projection reconstruction in figure 3(c) has clearly visible artifacts due to the irregular sampling, even though its mean spacing is at the Nyquist rate. The pseudo inverse reconstruction in figure 3(d) has no visible artifacts due to the irregular sampling.

## IV. ADVANCED IMAGE FORMATION FRAMEWORK

In this section we will present an advanced image formation framework using a mix of  $\ell_1$  and  $\ell_2$  regularisation, motivated by the theory of Compressed Sensing. The framework will be used to reconstruct the very bright targets  $f_s$  as well as the background  $f_{bg}$  from sub-sampled data. It will also include an iterative auto-focus method. Finally, the framework's ability to reconstruct  $f_s$  when compared to conventional techniques will be quantified using Automatic Target Recognition (ATR) rates.

### A. Compressed Sensing

CS theory states that a compressible signal can be well approximated from a significantly reduced number of samples compared to that which is required by the Nyquist-Shannon sampling theorem.

An under-sampled linear system  $\Phi$  is under-determined and from a traditional sampling perspective its inverse is ill-posed. However, if the vector to be recovered  $f$  is known to be approximately sparse it can accurately be approximated by solving the non-linear program (7) [23].

$$f = \arg \min_{\tilde{f}} \|\tilde{f}\|_1 \text{ subject to } \|y - \Phi \tilde{f}\| \leq \epsilon \quad (7)$$

Where,  $\epsilon$  is a small constant which allows for additive noise.

For the noiseless case, i.e.  $\epsilon = 0$ , it has been shown in [24] that by using the partial Fourier matrix for  $\Phi$ , equation (7) becomes equivalent to the sparse reconstruction problem with high probability. The partial Fourier matrix is a random  $m$  column subset of the  $n \times n$  discrete Fourier matrix. The  $\Phi$  matrix in randomly under-sampled SAR (the under-sampled re-projection matrix), through the Fourier slice theorem, is analogous to the partial Fourier matrix.

### B. Compressed Sensing for SAR

The reconstruction of the very bright targets  $f_s$  in a SAR image lends itself to the CS-framework because the features we are trying to reconstruct are sparse.

Using the CS framework  $f_s$  is reconstructed by equation (8).

$$f_s = \arg \min_{\tilde{f}} \|y - \Phi \tilde{f}\|_2^2 + \lambda \|\tilde{f}\|_1 \quad (8)$$

Where  $\lambda$  is a constant which controls the level of sparsity in the reconstructed image. Fast iterative solvers exist for equation (8) which can take advantage of fast (re/back)-projection [25]. This formulation has also been used for fully-sampled data in the context of superresolution [9], [10] due to its sharpening effect on the point spread function of very bright targets.

Since sparsity does not benefit the reconstruction of the speckled part of the image, we have to consider using non-sparsity based techniques. The simplest means to make the inversion well-posed is to use an  $\ell_2$  regularisation on the SAR image.  $f_{bg}$  is reconstructed by equation (9).

$$f_{bg} = \arg \min_{\tilde{f}} \|y_r - \Phi \tilde{f}\|_2^2 + \lambda \|\tilde{f}\|_2 \quad (9)$$

Where,  $y_r = y - \Phi f_s$  is the phase history with the very bright targets removed.

The reconstructed image using this inversion method still suffers from poor contrast and high speckle but has an improved image quality when compared to direct inversion methods. This improvement results from the energy of the very bright targets being removed. Using standard methods, the energy from the very bright targets is spread over the entire image, dominating the background of the image. Figure 4(a) and 4(b) demonstrate the visual improvement our framework provides when the phase history has been under-sampled.

### C. Auto-focus

In spotlight-mode SAR systems which use the dechirp-on-receive approach, the round trip propagation delay to the scene centre must be estimated. Errors in this estimate introduce unknown phase errors to the acquired data [26]. These phase errors can degrade and produce distortions in the reconstructed image.

Adding the delay error  $\tau_e$  into our SAR acquisition model, the received signal becomes

$$C_\theta(t) = \int_{-L}^{+L} p_\theta(u)P(u)P_{\tau_e}(t) \exp\left\{-j\frac{2u}{c}(\omega_0 + 2\alpha(t - \tau_0))\right\} du \quad (10)$$

Where,

$$P_{\tau_e}(t) = \exp\left\{-j(\omega_0\tau_e + \alpha\tau_e^2) - j2\alpha(t - \tau_0)\right\} \quad (11)$$

Equation (10) is the same as equation (3) except for an additional phase error term  $P_{\tau_e}(t)$ . The phase error term consists of a constant phase error  $-\omega_0\tau_e - \alpha\tau_e^2$  and a linear phase error  $-2\alpha(t - \tau_0)$ . The linear phase term produces a radial shift of  $\tau_e c/2$  in the range Fourier transformed phase history. If a SAR system's timing uncertainty is much less than the reciprocal of the chirp bandwidth  $\tau_e \ll 1/B$ , the linear phase term can be ignored [26]. This assumption may not be true for very large chirp-bandwidth systems.

Considering just the constant unknown phase error, classical auto-focus methods, such as the Phase Gradient Autofocus (PGA) method [27], indirectly use sparsity to correct phase errors. Using our framework sparsity can be directly used to correct phase errors by adding the errors into the reconstruction formulation, as in the following equation

$$(\phi, f_s) = \arg \min_{\tilde{\phi}, \tilde{f}} \|y - \Psi(\tilde{\phi})\Phi\tilde{f}\|_2^2 + \lambda\|\tilde{f}\|_1 \quad (12)$$

Where,  $\tilde{\phi} \in [-\pi, \pi]^m$  is a vector containing the estimated phase errors and  $\Psi$  is a diagonal matrix containing the elements  $e^{j\tilde{\phi}}$ . This program aims to concurrently solve the sparse image formation problem and the auto-focus problem. Like other classical auto-focus methods, this program is ambiguous for constant and linear phase errors. In most applications these ambiguities are benign. In [28] a very similar approach is used with fully-sampled synthetic data and images that contain no background.

Experimentally it was found that equation (12) could be solved approximately by iteratively minimising the objective using a single argument at a time in an alternating fashion. With  $\tilde{\phi}$  fixed, the program can be minimised using a fixed number of iterations of a fast iterative solver, in our results we use 5. With  $\tilde{f}$  fixed a direct solution for the program is obtained with almost negligible computation. It was found that with only a small number of iterations, in our examples 10, good approximations of  $f_s$  and  $\phi$  were obtained.

The values of  $R_\theta$  provided in the Gotcha data set contain significant differences to those calculated with the antenna positions provided. Errors in  $R_\theta$  have the same affect as timing errors do in the acquisition system. To accentuate the effects of phase errors on image reconstruction we have scaled the differences in  $R_\theta$  by a factor of four in the following results. Figure 4(c) and 4(d) shows reconstructions of the same 50% sub-sampled phase history with phase errors. Figure 4(c) was reconstructed using the framework proposed in section IV-B. Figure 4(d) was reconstructed with the same framework except using program (12) to reconstruct  $f_s$  and correct phase errors.

#### D. Automatic target recognition

We have shown that, compared with conventional imaging, the CS-enhanced system significantly improves the visual quality of SAR images. In this section, we quantify the image quality improvement by evaluating the automatic target recognition (ATR) performance. This is because the recognition process determines the target type of an object in a SAR image based on certain features, and obviously ATR performance depends on the image quality.

Usually a SAR image covers a large area and may have several targets. Hence, a detection process is required first to choose smaller

portions containing those targets from the large SAR image. Then a classifier realizes target recognition based on the small patch, which contains a possible target and some surrounding clutter. Man-made objects typically have much higher reflectivity in a SAR image than the surrounding clutter. Thus detection of possible targets could be done by comparing the magnitude of pixels to an appropriate threshold. We focus on the classification problem here and assume that the detection step is completed.

1) *Classifiers for ATR*: In this work we use the conventional mean-squared error (MSE) classifier [29], [30] for ATR. Given a set of reference images for each class the MSE classifier is a nearest neighbor classifier assigning the test image to the class that contains the closest reference image. The comparison is made between normalized magnitude images because variations in intensity and phase may occur for different SAR acquisition geometries. Also, before normalizing the images we set to zero all but the largest  $N_b$  pixels. This is because typically the brightest pixels are located within the target part, and the darker pixels constitute the clutter background and target shadow. Although the target shadow (the darkest pixels) contain information about the target which could be exploited to improve ATR performance, the value of the shadow pixels reconstructed from partial SAR data is not reliable.

Other classifiers have been proposed which may a priori perform well with partial data. Due to the space limitation, we only consider the MSE classifier in this paper since it provides the best performance. Interested readers may refer to [31] for more details.

2) *Simulation results*: In this section, simulation results are presented showing the ATR performance achieved by the MSE classifier. The classification performance based on the images reconstructed from the partial SAR data by the CS-enhanced system is compared with that based on the images recovered by the conventional back-projection approach, quantifying the image quality improvement brought in by the proposed scheme.

In the recognition simulation, we use images of BMP2 infantry fighting vehicles, BTR70 armored personnel carriers, and T72 tanks from the MSTAR public target database [32]. The database contains two types of images: small images containing only one vehicle and larger images containing only clutter. No raw data are available and the images are low-pass filtered. In order to simulate realistic raw data, we have mixed a vehicle image with a larger clutter image. To this end, we first invert the low-pass filtering for both images (following the procedure in [9]). The vehicle image is then superimposed to an empty region of the clutter image using cross-fading to blend the images smoothly. A sample field image (in dB) is shown in Fig. 2 (a). Given the mixed image, raw data are simulated using the (fast) re-projection algorithm described in section IV. The SAR data are then subsampled along the aperture, either uniformly at random or by removing a chunk of data in the middle of the aperture (see Fig. 2 (b) and (c)). The second subsampling pattern can be interpreted as temporary interruption of data acquisition. Sample images recovered from 25% subsampled SAR data by using the CS-enhanced system and conventional approach are presented in Fig. 2. Given the reconstructed image, we choose the small patch containing the target (detection step) and implement ATR by following the classification procedure described in the previous section.

We choose a set of 687 images of the BMP2, BTR70, and T72 targets at  $17^\circ$  elevation angle as the reference image set and an independent set of 200 images at  $15^\circ$  elevation angle as the test image set. The classification decision is made for every image in the test set, and the ATR performance is evaluated by the probability of correct classification  $\text{Pr}_{cc}$ , which is the percentage of all test targets that are correctly recognized. Table II shows the recognition rates based on the CS-enhanced and conventional back-projection images

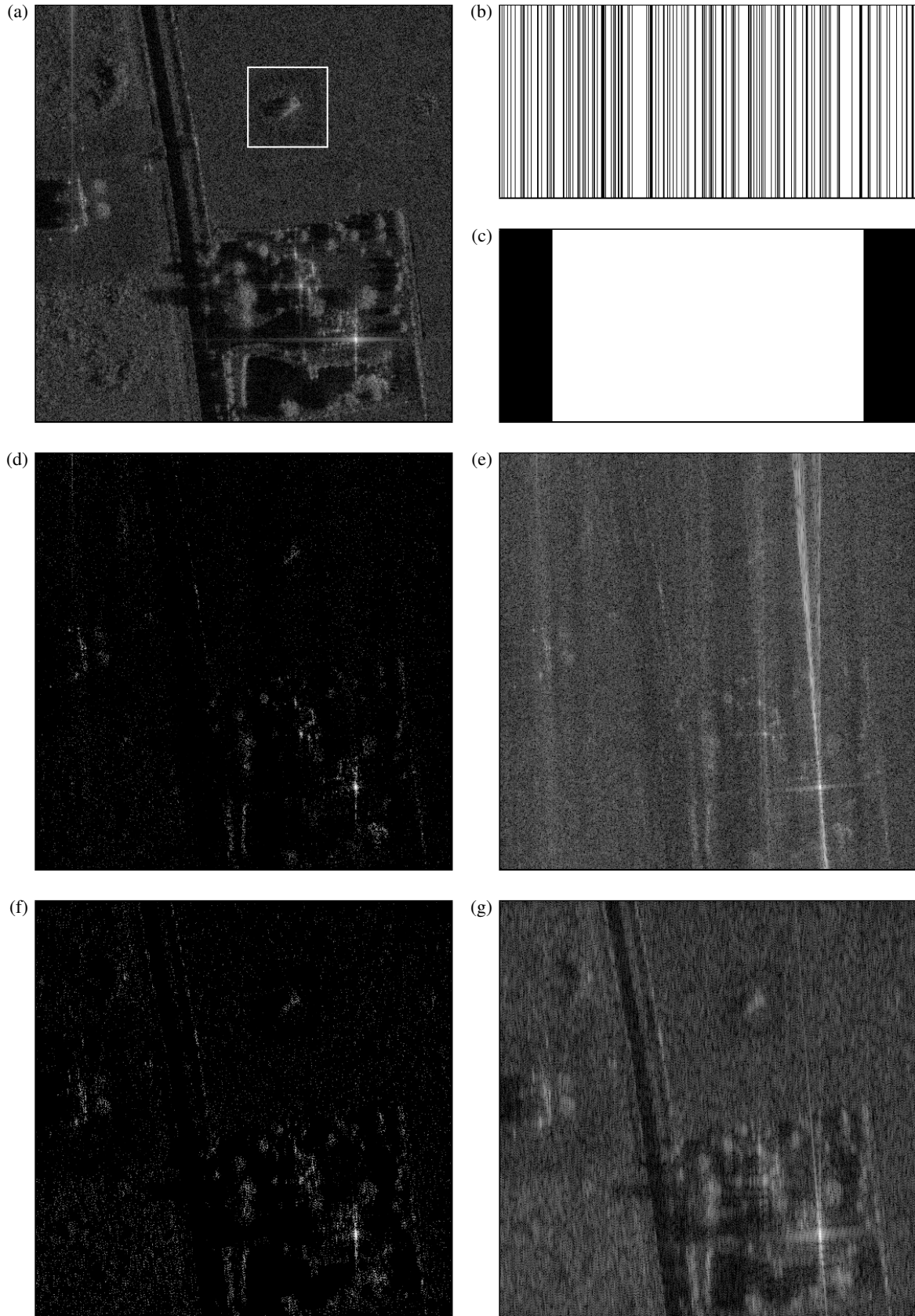


Fig. 2. (a) Original synthetic SAR image. The white square indicates the target area. (b) and (c) “random” and “gap” subsampling patterns respectively. (d) and (f) CS-enhanced images reconstructed from 25% subsampled data with patterns (b) and (c) respectively (sparse coherent part only). (e) and (g) Back-projection images reconstructed from 25% subsampled data with patterns (b) and (c) respectively. (Images are in logarithmic scale with 65 dB dynamic range.)

reconstructed from full and partial SAR raw data.

TABLE II  
ATR PERFORMANCE OF DIFFERENT SCENARIOS ( $Pr_{cc}$ )

missing data pattern	data amount	CS-framework	back-projection
	full data	96.5%	95.5%
random	25% data	93%	85.5%
	10% data	83%	69%
gap	25% data	82%	64%
	10% data	57%	40.5%

The simulation results show that for every considered scenario, images reconstructed by the CS-enhanced system lead to better ATR performance than that of the conventional recovered images. With randomly subsampled data, the CS-enhanced system slightly decreases the ATR performance when only 25% data, instead of full raw data, are known. High recognition rates can even be achieved when only a small percentage of raw data is available (e.g., 10% data). The back-projection approach performs much worse because it suffers from strong sidelobes as shown in Fig. 2 (e). For the gapped data scenario, the aliasing effect degrades the recognition performance of both approaches. However, CS-enhanced system still significantly improves ATR performance compared with the back-projection method, and it can realize good recognition performance with 25% data only.

## V. CONCLUSIONS

In this paper we have shown that advanced SAR image formation frameworks, based on iterative algorithms that utilise fast (re/back)-projection operators, are not computationally unrealistic. Since high quality reconstructions can be achieved with a small number of iterations, the complexity of iterative techniques, when compared to standard techniques, is only increased by a constant factor. The development of parallel implementations of the fast (re/back)-projection operators on Graphics Processing Units (GPU) has further increased the feasibility of iterative frameworks and makes this work timely [33]. In certain imaging scenario, such as under-sampled data, iterative algorithms could play an important role in future generations of SAR image formation processors.

## REFERENCES

- [1] L. Greengard and J.-Y. Lee, "Accelerating the nonuniform fast Fourier transform," *SIAM Review*, vol. 46, no. 3, pp. 443–454, 2004. [Online]. Available: <http://link.aip.org/link/?SIR/46/443/1>
- [2] S. Xiao, D. Munson, S. Basu, and Y. Bresler, "An  $N^2 \log N$  Back-Projection Algorithm for SAR Image Formation," in *Asilomar Conference on Signals Systems and Computers*, vol. 1. IEEE; 1998, 2000, pp. 3–7.
- [3] D. Wahl, D. Yocky, and C. Jakowatz Jr, "An implementation of a fast backprojection image formation algorithm for spotlight-mode SAR," in *Proceedings of SPIE*, vol. 6970, 2008, p. 69700H.
- [4] L. Demanet, M. Ferrara, N. Maxwell, J. Poulson, and L. Ying, "A butterfly algorithm for synthetic aperture radar imaging," (submitted).
- [5] J. Salzman, D. Akamine, R. Lefevre, and J. Kirk, J.C., "Interrupted synthetic aperture radar (SAR)," *IEEE Trans. Aerosp. Electron. Syst.*, vol. 17, no. 5, pp. 33–39, may 2002.
- [6] A. Doerry, F. Dickey, and L. Romero, "Windowing Functions for SAR data with spectral gaps," in *Proceedings of SPIE*, vol. 5095, 2003, p. 54.
- [7] S. Bhattacharya, T. Blumensath, B. Mulgrew, and M. Davies, "Fast encoding of synthetic aperture radar raw data using compressed sensing," in *IEEE Work. Statist. Signal Process.*, Madison, USA, August 2007.
- [8] G. Rilling, M. E. Davies, and B. Mulgrew, "Compressed sensing based compression of SAR raw data," in *Proceedings of SPARS'09*. Saint-Malo (F), Apr. 2009.
- [9] M. Çetin, "Feature-enhanced synthetic aperture radar imaging," Ph.D. dissertation, Boston University, 2001.
- [10] M. Ferrara, J. Jackson, and C. Austin, "Enhancement of multi-pass 3D circular SAR images using sparse reconstruction techniques," in *Algorithms for Synthetic Aperture Radar Imagery XVI, EG Zelnio and FD Garber, eds., SPIE Defense and Security Symposium,(Orlando, FL)*. Citeseer, 2009.
- [11] M. Çetin and R. L. Moses, "Synthetic aperture radar imaging from wide-angle data with frequency-band omissions," in *IEEE 14th Signal Process. and Commun. App.*, 17-19 2006, pp. 1–4.
- [12] G. Rilling, C. Du, M. E. Davies, and M. Bernard, "Processing sar data with gaps in the aperture: A compressed sensing perspective," in *Proceedings of International Conference on Synthetic Aperture Sonar and Synthetic Aperture Radar*, September 2010, lerici (I).
- [13] E. J. Candes, J. Romberg, and T. Tao, "Robust uncertainty principles: exact signal reconstruction from highly incomplete frequency information," *IEEE Trans. Inf. Theory*, vol. 52, no. 2, pp. 489–509, Feb. 2006.
- [14] Y. Tsaig and D. L. Donoho, "Compressed sensing," *IEEE Trans. Inf. Theory*, vol. 52, no. 4, pp. 1289–1306, 2006.
- [15] M. Figueiredo, R. Nowak, and S. Wright, "Gradient projection for sparse reconstruction: Application to compressed sensing and other inverse problems," *IEEE J. Sel. Topics Signal Process.*, vol. 1, no. 4, pp. 586–597, Dec. 2007.
- [16] E. van den Berg and M. P. Friedlander, "Probing the Pareto frontier for basis pursuit solutions," *SIAM J. Sci. Comput.*, vol. 31, pp. 890–912, Nov. 2008.
- [17] D. Munson Jr, J. O'brien, and W. Jenkins, "A Tomographic Formulation of Spotlight-Mode Synthetic Aperture Radar," *Proceedings of the IEEE*, vol. 71, no. 8, pp. 917–925, 1983.
- [18] Y. Dong, B. Förster, and C. Ticehurst, "Radar backscatter analysis for urban environments," *International Journal of Remote Sensing*, vol. 18, no. 6, pp. 1351–1364, 1997. [Online]. Available: <http://www.informaworld.com/10.1080/014311697218467>
- [19] L. Ulander, H. Hellsten, and G. Stenstrom, "Synthetic-aperture radar processing using fast factorized back-projection," *Aerospace and Electronic Systems, IEEE Transactions on*, vol. 39, no. 3, pp. 760–776, 2003.
- [20] W. Carrara, R. Goodman, and R. Majewski, *Spotlight Synthetic Aperture Radar - Signal Processing Algorithms*. Artech House, 1995.
- [21] D. C.-L. Fong and M. A. Saunders, Lsmr: an iterative algorithm for sparse least-squares problems, month = jun, year = 2010, url = <http://arxiv.org/abs/1006.0758>.
- [22] C. H. Casteel Jr, L. A. Gorham, M. J. Minardi, S. M. Scarborough, K. D. Naidu, and U. K. Majumder, "A challenge problem for 2D/3D imaging of targets from a volumetric data set in an urban environment," in *SPIE Algorithms for Synthetic Aperture Radar Imagery XIV*, 2007.
- [23] E. Candes and T. Tao, "Near-optimal signal recovery from random projections: Universal encoding strategies?" *Information Theory, IEEE Transactions on*, vol. 52, no. 12, pp. 5406–5425, 2006.
- [24] M. Rudelson and R. Vershynin, "On sparse reconstruction from Fourier and Gaussian measurements," *Communications on Pure and Applied Mathematics*, vol. 61, no. 8, pp. 1025–1045, 2008.
- [25] M. Figueiredo, R. Nowak, and S. Wright, "Gradient projection for sparse reconstruction: Application to compressed sensing and other inverse problems," *Selected Topics in Signal Processing, IEEE Journal of*, vol. 1, no. 4, pp. 586–597, 2008.
- [26] C. Jakowatz, D. Wahl, P. Eichel, G. D.C., and P. Thompson, *Spotlight-mode synthetic aperture radar: a signal processing approach*. Kluwer Academic Pub, 1996.
- [27] D. Wahl, P. Eichel, D. Ghiglia, and C. Jakowatz Jr, "Phase gradient autofocus-a robust tool for high resolution SAR phase correction," *Aerospace and Electronic Systems, IEEE Transactions on*, vol. 30, no. 3, pp. 827–835, 2002.
- [28] N. Onhon and M. Çetin, "A Nonquadratic Regularization-based Technique for Joint SAR Imaging and Model Error Correction," in *Proceedings of SPIE*, vol. 7337, 2009, p. 73370C.
- [29] L. M. Novak, S. D. Halversen, G. Owirka, and M. Hiatt, "Effects of polarization and resolution on SAR ATR," *Aerospace and Electronic Systems, IEEE Transactions on*, vol. 33, no. 1, pp. 102–116, Jan. 1997.
- [30] M. Çetin, W. C. Karl, and D. A. Castanon, "Feature enhancement and ATR performance using nonquadratic optimization-based SAR imaging," *IEEE Trans. Aerosp. Electron. Syst.*, vol. 39, no. 4, pp. 1375–1395, Oct. 2003.
- [31] C. Du, G. Rilling, M. Davies, and B. Mulgrew, "Automatic target recognition from highly incomplete SAR data," in *Algorithms for synthetic aperture radar imagery XVIII*, ser. Proc. SPIE, Orlando, Florida, Apr. 2011.
- [32] [Online]. Available: <https://www.sdms.afrl.af.mil/index.php?collection=mstar/>

- [33] A. Rogan and R. Carande, "Improving the fast back projection algorithm through massive parallelizations," in *Proceedings of SPIE*, vol. 7669, 2010, p. 76690I.

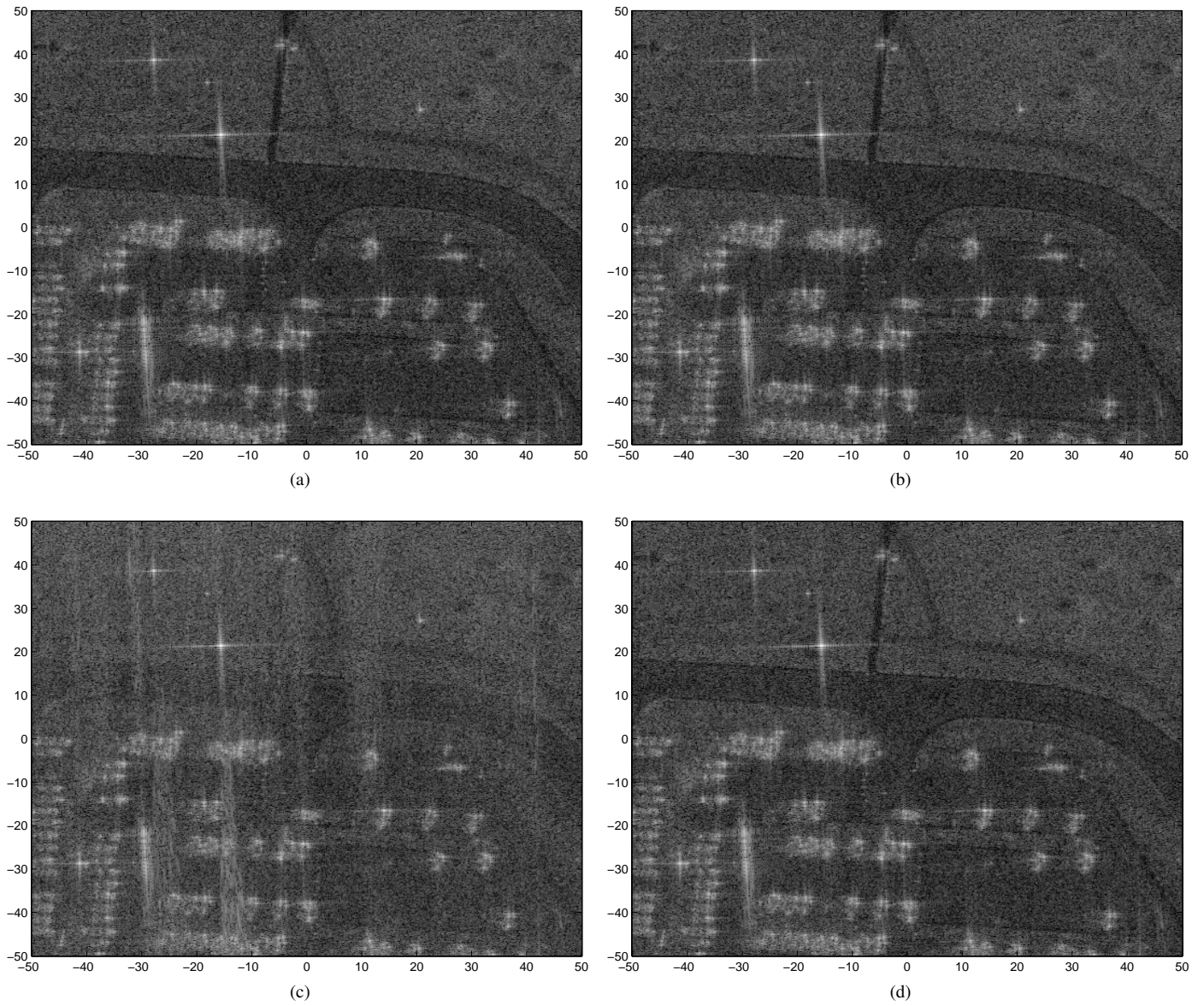


Fig. 3. Image formation using  $4^\circ$  of fully-sampled data of the Gotcha data set. (a) Standard back-projection reconstruction. (b) Fast back-projection reconstruction. (c) Fast back-projection reconstruction with irregularly spaced projections. (d) Approximate pseudo inverse reconstruction with irregularly spaced projections.

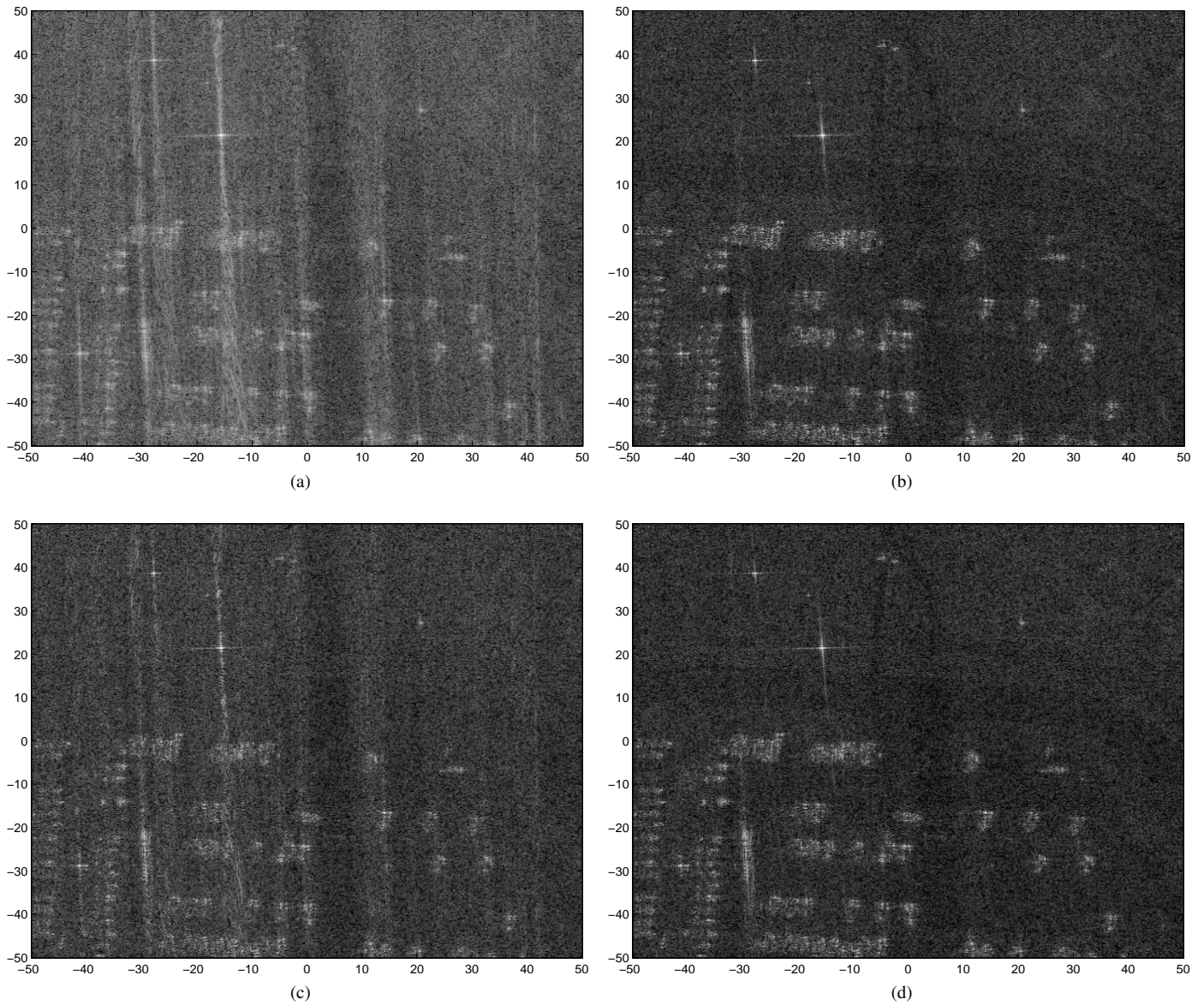


Fig. 4. Image formation using  $4^\circ$  of the Gotcha data set, 50% uniform randomly under-sampled in cross-range. (a)  $\ell_2$  regularised LS reconstruction. (b) Mixed  $\ell_1/\ell_2$  regularised LS reconstruction. (c) Mixed  $\ell_1/\ell_2$  regularised LS reconstruction with phase errors. (d) Mixed  $\ell_1/\ell_2$  regularised LS reconstruction with phase errors using auto-focus.